Scattering at the ultrastrong: nonlinear optics with one photon Supplementary Material

E. Sanchez-Burillo,[1] D. Zueco,[1,2] J. J. Garcia-Ripoll,[3] and L. Martin-Moreno[1]

[1] *Instituto de Ciencia de Materiales de Aragon and Departamento de Fisica de la Materia Condensada, CSIC-Universidad de Zaragoza, E-50012 Zaragoza, Spain*

[2] *Fundacion ARAID, Paseo Maria Agustin 36, E-50004 Zaragoza, Spain*

[3] *Instituto de Fisica Fundamental, IFF-CSIC, Calle Serrano 113b, Madrid E-28006*

This supplementary material is structured in sections: (i) reviews the MPS technique, (ii) checks the convergence of the algorithm, (iii) provides details of the simulations, (iv) studies the frequency shift of the transmission minimum (v) presents representative cases for the time evolution of the qubit population, (vi) estimates the effect of dissipation by studying a model where the qubit is coupled to a second waveguide, and (vii) shows a theorem saying that it is not possible to have frequency conversion with linear systems and a single photon as input.

I. MATRIX PRODUCT STATES

As we indicated in the letter, we solve the problem by using the MPS technique. Let us justify why we can do it.

Unlike in [1], our bandwidth-limited photonic medium can be treated in the RWA and its ground state is the vacuum both in frequency and position space. Moreover, even if we go beyond RWA in the qubit-resonator coupling ($g/\Delta \gtrsim 0.1$), it is true that the ground state is not the vacuum anymore, as we show in the paper, but it will follow the area law [2], so it will be slightly entangled. As we are studying the dynamics of a photon flying over the ground state, the state will have a small amount of entanglement.

The important consequence of the previous discussion is that we may use the variational ansatz of Matrix Product States [3, 4] to describe the discrete wavefunction, since it is valid for 1D systems when the entanglement is small enough. This ansatz has the form

$$|\psi\rangle = \sum_{s_i \in \{1,d_i\}} \mathrm{tr}\left[\prod A_i^{s_i}\right] |s_1, s_2, \ldots, s_L\rangle \,. \tag{1}$$

It is constructed from L sets of complex matrices $A_i^{s_i} \in M[\mathbb{C}^D]$, where each set is labeled by the quantum state s_i of the corresponding site. The local Hilbert space dimension d_i is infinity, since we are dealing with bosonic sites. However, during the dynamics, processes that create multiple photons are still highly off-resonance. Then, we can truncate the bosonic space and consider states with 0 to n_{max} photons per cavity. So, the composite Hilbert space is $\mathcal{H} = \bigotimes_i \mathbb{C}^{d_i}$, where the dimension is $d_i = n_{max} + 1$ for the empty resonators and $d_{i_0} = 2(n_{max} + 1)$ for the cavity with the qubit. We thus expect the composite wavefunction of the photon-qubit system to consist of a superposition with a small number of photons

The total number of variational parameters $(L-1)D^2(n_{max}+1) + 2D^2(n_{max}+1)$ depends on the size of the matrices, D. The key point is that, for describing a general state, D increases exponentially with L, whereas its dependence is polynomial if the entanglement is small enough, in such a way that the number of parameters increases polynomially with L for this class of states.

Our work with MPS relies on four different algorithms. The most basic one is to create trivial, product states of known shape, such as a vacuum state with a de-excited qubit $|\psi\rangle = |\downarrow\rangle\,|vac\rangle$. These states can be reproduced using matrices of bond dimension $D = 1$, so each matrix is just a coefficient $A_i^{s_i} = \delta_{s_i 1}$. The second algorithm is to compute expectation values from MPS. This amounts to a contraction of tensors that can be performed efficiently [3], and allows us to compute single-site operators $\langle a_i^\dagger a_i\rangle$, $\langle \sigma_z\rangle$, or correlators, $\langle a_i^\dagger a_j\rangle$. The third operation that we need to perform is to apply operators on to the state, $O\,|\psi\rangle$, such as introducing or removing excitations $a_i^\dagger\,|\psi\rangle$. We do this in an efficient fashion by interpreting the operator O as a Matrix Product Operator (MPO) [5]. A MPO is a matrix product representation of an operator:

$$O = \sum_{s_i, s_i' \in \{1,d_i\}} \mathrm{tr}\left[\prod B_i^{s_i, s_i'}\right] |s_1, s_2, \ldots, s_L\rangle\,\langle s_1', s_2', \ldots, s_L'| \tag{2}$$

So, now we have L sets of complex matrices $B_i^{s_i, s_i'} \in M[\mathbb{C}^{D_O}]$, where each set is labeled by two indices s_i, s_i' of the corresponding site.

We just need to apply sums of one-body operators

$$O = a_\phi^\dagger = \sum_n \phi_n a_n^\dagger. \tag{3}$$

In such a case, an efficient representation of the MPO is obtained with $D_O = 2$

$$B_i^{s_i,s_i'} = \begin{pmatrix} \delta_{s_i,s_i'} & 0 \\ \phi_i(a_i^\dagger)_{s_i,s_i'} & \delta_{s_i,s_i'} \end{pmatrix} \qquad i = 2, 3, \ldots, L-1, \tag{4}$$

whereas $B_1^{s_1,s_1'} = (\phi_1(a_1^\dagger)_{s_1,s_1'}, \delta_{s_1,s_1'})$ and $B_L^{s_L,s_L'} = (\delta_{s_L,s_L'}, \phi_L(a_L^\dagger)_{s_L,s_L'})^T$, with $(a_i^\dagger)_{s_i,s_i'} =: \langle s_i | a_i^\dagger | s_i' \rangle$.

Finally, with this tool in our box, we can also approximate time evolution, repeatedly contracting the state with an MPO approximation of the unitary operator $\exp(-iH\Delta t)$ for short times, and truncating it to an ansatz with a fixed D. Since our problem does not contain long-range interactions and since the state is well approximated by MPS, it is sufficient to rely on a third-order Suzuki-Trotter formula [6]. In the same way as we can consider time evolution, we can take imaginary time to obtain the ground state and excited states, that is solving the equation $i\frac{d}{dt}P|\psi\rangle = PHP|\psi\rangle$ for finite time-steps, while constantly renormalizing the state. Here, P is either the identity (for the ground state) or a projector that either selects a well defined quantum number (parity Π) or projects out already computed states. In either case, provided a suitable initial state, the algorithm converges to the lowest-energy state of PHP in the subspace selected by P. Note that, while the excited states are useful in order to interpret the results, the ground state is totally necessary to study the dynamics, since our initial state is just a photon flying over the ground state.

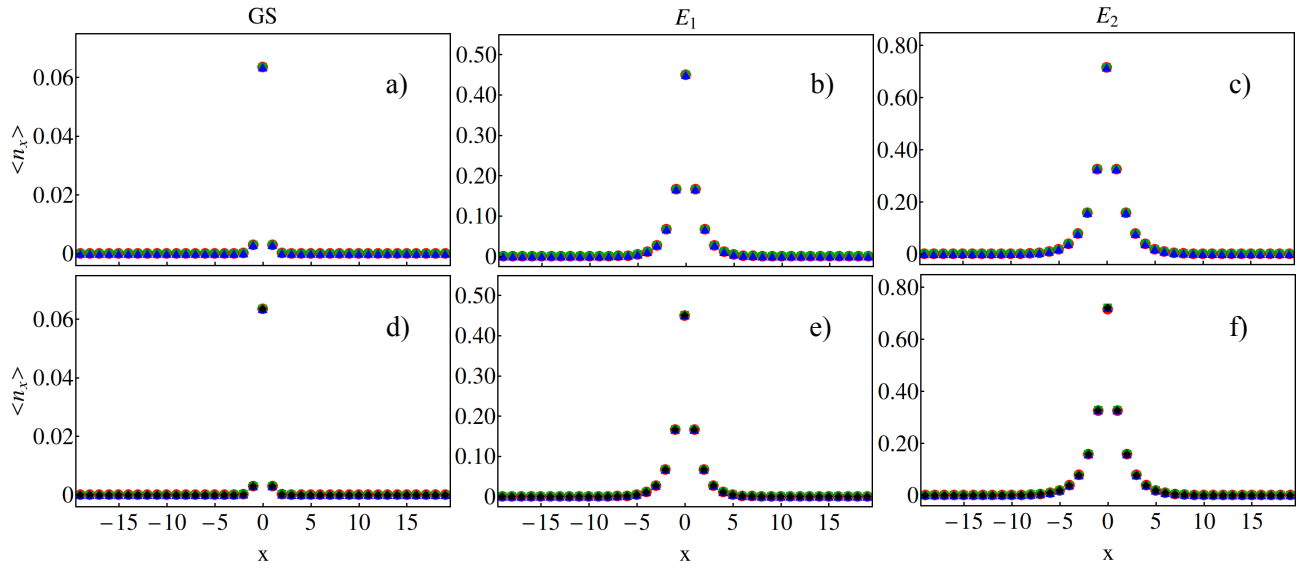

FIG. 1. **Convergence of $\langle n_x \rangle$.** *(Color online).* For the representative value $g/\Delta = 0.4$, this figure shows $\langle n_{max} \rangle$ as function of position in the chain, for the ground state (left column), the first excited state (middle column) and the second excited state (right column). In the first row we fix $n_{max} = 4$ and consider the cases $D = 6$ (red circles), $D = 10$ (green squares) and $D = 14$ (blue triangles). In the second row, we fix $D = 10$ and consider $n_{max} = 4$ (red circles), $n_{max} = 5$ (green squares), $n_{max} = 6$ (blue triangles) and $n_{max} = 7$ (black diamonds). These results show that considering $n_{max} = 4$ and $D = 10$ already provides converged results for this value of g/Δ.

II. CHECKING CONVERGENCE OF THE ALGORITHM

In this section we check the convergence of the algorithm. We compute the number of excitations per site $\langle n_x \rangle$ for the ground state, the first and the second excited states and the transmission probability, for several values of the variational parameters: the bond dimension D and the cutoff in the number of excitations per site n_{max}.

We show $\langle n_x \rangle$ in the figures 1 and 2 for the ground (GS, first column), first excited (E_1, second column) and second excited (E_2, third column) states, for the representative cases of $g = 0.4$ and $g = 0.7$ respectively. For results in the

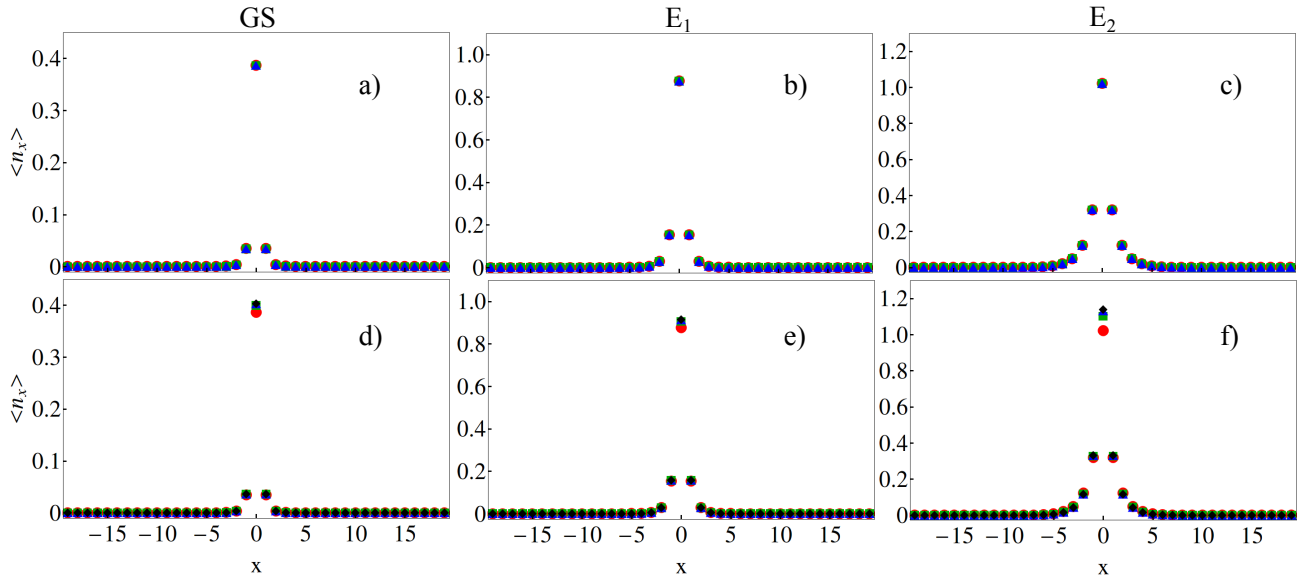

FIG. 2. **Convergence of $\langle n_x \rangle$.** *(Color online)* This figure study the convergence of the three lowest-lying energy eigenstates with both D and n_{max} for $g/\Delta = 0.7$. All other parameters are like in Fig. 1. As seen in the first row, the convergence in D is fast for the ground state. In the second row, although there are small differences among the results for different values of n_{max}, the convergence is good even for moderate n_{max}.

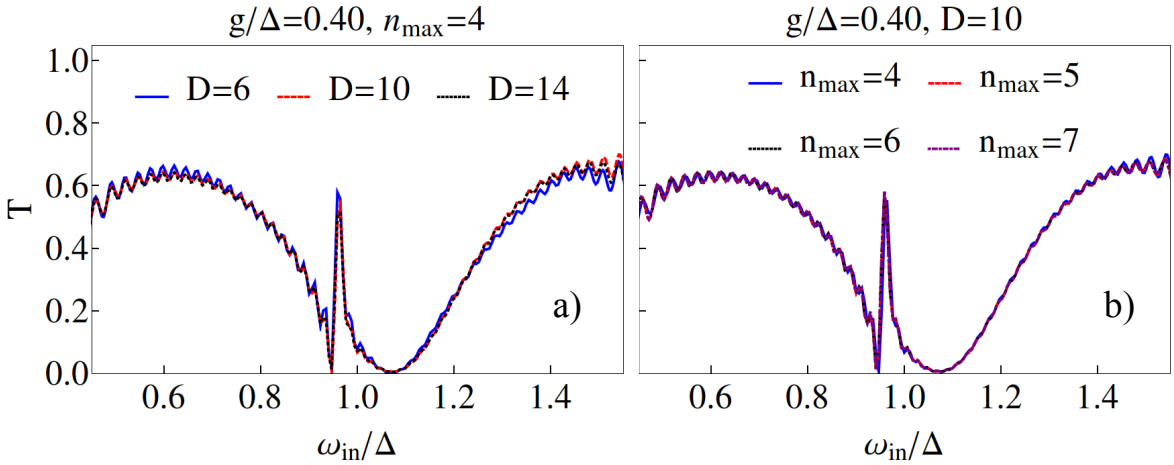

FIG. 3. **Convergence of T.** (*Color online)* For the representative value $g/\Delta = 0.4$, Panel (a) studies the convergence of T on bond dimension for $D = 6$ (blue, solid), $D = 10$ (red, dashed) and $D = 14$ (black, dotted). Panel (b) shows the convergence on n_{max}, for $n_{max} = 4$ (blue, solid), $n_{max} = 5$ (red, dashed), $n_{max} = 6$ (black, dotted) and $n_{max} = 7$ (purple, dotted-dashed). In accordance with what was found for the convergence on n_{max}, the transmittance converges quickly on both D and n_{max} for this value of g/Δ.

first row we fix $n_{max} = 4$, and consider $D = 6, 10, 14$. In the second row, we fix $D = 10$ and take $n_{max} = 4, 5, 6, 7$. As seen, the curves converge with both parameters; there are just little differences when modifying n_{max} for $g = 0.7$.

Figures 3 and 4 show the transmission spectra for $g = 0.4$ and $g = 0.7$, respectively, for a fixed $n_{max} = 4$ and the same values of D as before (left panel). In the right panel we fix $D = 10$ and take those values of n_{max} we considered in the previous figures. As we see, for $g = 0.4$ the curves hardly change for these values of D and n_{max} in all the frequency range, so the convergence is good already for $n_{max} = 4$ and $D = 10$. For $g = 0.7$, we need D to be large enough, since we even obtain unphysical values $T > 1$ at the Fano-like resonance if $D = 6$. On the other hand, the position of the Fano peak slightly depends on n_{max}, but it has virtually converged for $n_{max} = 5$ and the main physics is already captured for $n_{max} = 4$.

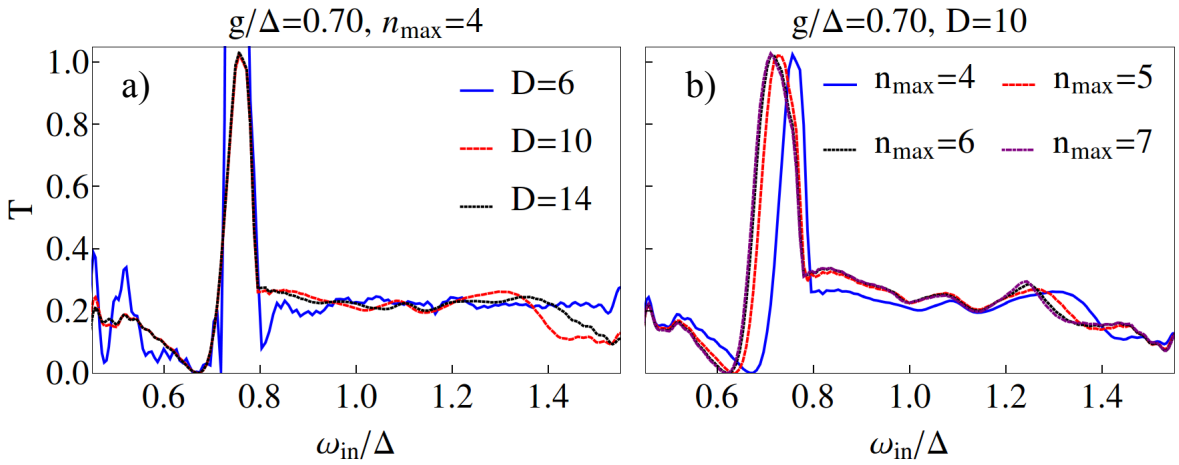

FIG. 4. **Convergence of T.** (*Color online)* This figure shows the same cases as Fig. 3, but this time for $g/\Delta = 0.7$.

III. DETAILS OF THE SIMULATIONS

We took chains of $L = 480$ cavities, with the qubit interacting with the cavity placed at $j = 240$ and the incident wave packet centered at $j = 160$, except for the inset of the figure 5, where we placed the qubit interacting with the cavity at $j = 460$ and the incident wave packet centered at 380. The results of the figures 3 and 6 were done with $n_{max} = 4$ and $D = 10$. The width of the incident wave packet of the figures 4 and 5 is $\sigma = 2$ (narrow in positions, broad in momenta, to compute the transmission factor for a large range of energies), whereas for the figures 3 and 6 we took $\sigma = 20$, to see the dynamics of photons with well defined momentum. We took a total time $t = 420$ in all the simulations, but in the inset of the figure 5, where we took $t = 800$, since that wavepacket between the qubit and the wall goes back and forth again and again.

IV. FREQUENCY SHIFT

In this section we show that it is possible to describe properly the frequency shift with an approximate calculation. First of all, we consider that the scatterer is the cavity-qubit system and we truncate its Hilbert space just to the ground state and the couple of states which have just one particle in the low coupling regime, that is, the polariton states, which in RWA are

$$|e_\pm\rangle = (a_0^\dagger|0\rangle \pm \sigma^+|0\rangle)/\sqrt{2}. \tag{5}$$

Then, a general state in this subspace is

$$|\Psi\rangle = \sum_{n\neq 0} c_n a_n^\dagger|GS\rangle + f_+|\tilde{e}_+\rangle + f_-|\tilde{e}_-\rangle, \tag{6}$$

where $\{|\tilde{e}_i\rangle\}$ are the polariton states calculated beyond the RWA for a system comprising just one cavity plus one qubit. Taking the following ansatz we can find the scattering eigenstates

$$c_n = \begin{cases} e^{ikn} + r_k e^{-ikn} & n < 0 \\ t_k e^{ikn} & n > 0 \end{cases} \tag{7}$$

Solving the eigenvalue equation $H\,|\Psi\rangle = E\,|\Psi\rangle$, we show that the transmission amplitude is

$$t_k = \frac{2iG\sin k}{2e^{ik}G - 1}, \qquad G := J\sum_{i=\pm}\frac{|\alpha_{i0}|^2}{\Delta_i - \omega_k}. \tag{8}$$

Here, Δ_i is the gap between $|\tilde{e}_i\rangle$ and $|GS\rangle$ and $\alpha_{i0} = \langle\tilde{e}_i|a^\dagger|GS\rangle$. By imposing $t_k = 0$, we find that the resonant energy for perfect reflection is

$$\omega_R = \frac{|\alpha_{+0}|^2\Delta_- + |\alpha_{-0}|^2\Delta_+}{|\alpha_{+0}|^2 + |\alpha_{-0}|^2}. \tag{9}$$

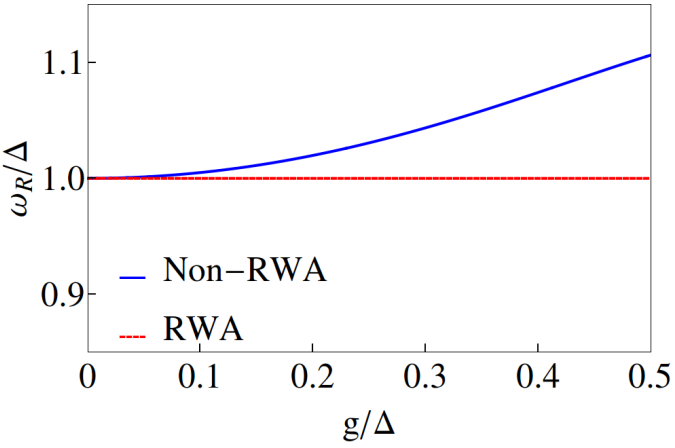

FIG. 5. **Resonant energy for perfect reflection.** ω_R shifts to larger values as g increases when computed beyond the RWA (blue, solid line), whereas it remains constant within the RWA (red, dashed line).

In the RWA, $\alpha_{\pm 0} = 1/\sqrt{2}$, and $\Delta_\pm = \Delta \pm g$, so $\omega_R = \Delta$. However, counter rotating terms modify both the gaps and the matrix elements, so the resonant frequency shifts, as we plot in the figure 5. In the manuscript, the same curve is plotted over the figure 4.b, and it fits really well with the numerical result obtained with MPS. A deeper study of this method will be shown elsewhere.

V. TIME EVOLUTION OF QUBIT POPULATION.

The excitation of dressed-qubit bound states have a strong impact on the dynamics of the qubit excited state population P. Figure 6 shows, for several values of the coupling g, the time evolution of $\Delta P = P - P_{GS}$ (where P_{GS} is evaluated on the GS) for an incoming one-photon wave packet with a representative $\omega_{in} = 0.9$. For $g < 0.3$, the qubit dynamics is governed by the excitation by the passing wave packet and the fast de-excitation of the qubit. For $0.3 < g < 0.55$, ΔP shows a slow decay characterized by multi-exponential relaxations, associated to the resonant excitation of both E_3 and E_2 (which is a virtual process in this range). For higher g, the Raman excitation becomes a real process and ΔP is finite at long times.

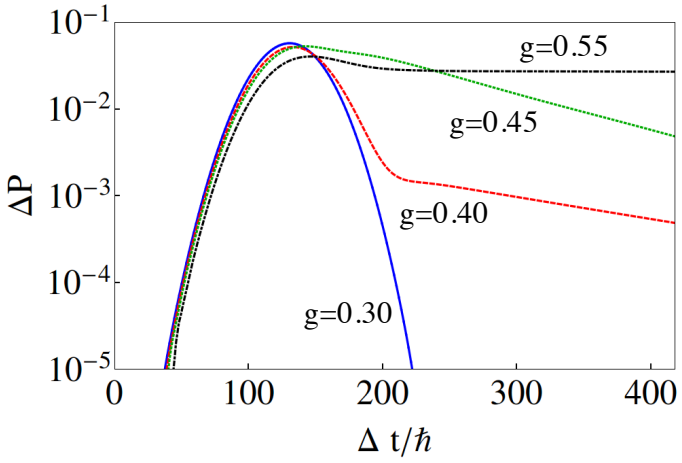

FIG. 6. **Qubit dynamics.** Time evolution for the population of the qubit excited state, with respect to that in the ground state, for $\omega_{in} = 0.9$ and several values of the photon-qubit coupling g. The wave packet width is $\sigma = 20$, for which $|\delta\omega_{in}/4J| \simeq 0.04 \ll 1$. While for $g = 0.3$ (solid) the time dynamics corresponds to a fast decay back to the GS, multi-relaxation long-lived process occur for $g = 0.4$ (dashed) and 0.45 (dotted). At $g = 0.55$ (dashed-dotted) Raman scattering is energetically possible and the qubit ends up in an excited stationary state.

VI. INFLUENCE OF DISSIPATION IN THE QUBIT

In order to estimate the influence of dissipation in the transmission processes discussed in the main text, we have considered the scattering of one photon by one qubit, when the qubit is connected to a second (upper) chain, with coupling strength g' (see the sketch of the considered geometry in Fig. 7 a)). This second chain acts as a lossy channel for the photons moving in the lower chain. In the weak coupling regime, this way of treating dissipation is equivalent to the usual treatment in quantum optics using master equations[7].

The Hamiltonian for the whole system is now:

$$\begin{aligned} H =&\epsilon \sum_n a_n^\dagger a_n - J\sum_n (a_n^\dagger a_{n+1} + hc) + \Delta\sigma^+\sigma^- + g\sigma_x(a_0 + a_0^\dagger) \\ &+\epsilon \sum_n b_n^\dagger b_n - J\sum_n (b_n^\dagger b_{n+1} + hc) + g'\sigma_x(b_0 + b_0^\dagger), \end{aligned} \tag{10}$$

where $\{b_n\}$ in the set of annihilation operators in the second chain.

This model can be related to the one-chain model that we consider in the text, by using the canonical bosonic transformation

$$\begin{pmatrix} \alpha_n \\ \beta_n \end{pmatrix} = \frac{1}{\sqrt{1+(g'/g)^2}} \begin{pmatrix} 1 & g'/g \\ g'/g & -1 \end{pmatrix} \begin{pmatrix} a_n \\ b_n \end{pmatrix}, \tag{11}$$

In terms of the new bosonic operators the Hamiltonian reads

$$H = \epsilon \sum_n (\alpha_n^\dagger \alpha_n + \beta_n^\dagger \beta_n) - J\sum_n (\alpha_n^\dagger \alpha_{n+1} + \beta_n^\dagger \beta_{n+1} + hc) + \Delta\sigma^+\sigma^- + \sqrt{g^2+(g')^2}\sigma_x(\alpha_0 + \alpha_0^\dagger) \tag{12}$$

So, the problem has been mapped into two independent chains: (i) a free chain (the one with the set of operators $\{\beta_n\}$), with no qubit present and (ii) a chain (that of the α_n's) interacting with one qubit, with a "renormalized" coupling $\hat{g} = \sqrt{g^2+(g')^2}$. Finding the wave function in the first case is trivial, while the second problem is precisely the one that we consider in the manuscript, so we can relate the case with dissipation to that without losses. Notice that the transformation is valid for any value of the coupling strengths g and g', so the mapping remains valid in the ultra-strong regime.

In order to find the scattering coefficients, we express the initial wavefuncion in terms of the new bosonic operators:

$$|\Psi_{in}\rangle = \sum_n \phi_n a_n^\dagger |GS\rangle = \sum_{k>0} \tilde{\phi}_k a_k^\dagger |GS\rangle = \frac{1}{\sqrt{1+(g'/g)^2}} \sum_{k>0} \tilde{\phi}_k(\alpha_k^\dagger + (g'/g)\beta_k^\dagger)|GS\rangle, \tag{13}$$

Where $\tilde{\phi}_k$ is the Fourier transform of ϕ_n. The wavefunction after the scattering has occurred can be expressed in terms of the previously computed transmission and reflection coefficients, t_k and r_k, respectively:

$$|\Psi_{out}\rangle = \frac{1}{\sqrt{1+(g'/g)^2}} \sum_{k>0} \tilde{\phi}_k(t_k(\hat{g})\alpha_k^\dagger + r_k(\hat{g})\alpha_{-k}^\dagger + (g'/g)\beta_k^\dagger)|GS\rangle + \frac{1}{\sqrt{1+(g'/g)^2}} \sum_k \phi_k t_{2,k}(\hat{g})\alpha_{k'}^\dagger|\text{exc}\rangle \tag{14}$$

Here $t_{2,k}$ is amplitude probability to leave the qubit in an excited state after the scattering, $|\text{exc}\rangle$ is the excited state involved in this Raman process and k' is the new photon momentum fulfilling energy conservation, $\omega_{k'} + E_{\text{exc}}(\hat{g}) = \omega_k + E_{GS}(\hat{g})$. Transforming back to the original bosonic operators, defined in the real chains:

$$\begin{aligned} |\Psi_{out}\rangle =&\frac{1}{1+(g'/g)^2} \sum_{k>0} \tilde{\phi}_k((t_k(\hat{g}) + (g'/g)^2)a_k^\dagger + r_k(\hat{g})a_{-k}^\dagger + (g'/g)(t_k(\hat{g}) - 1)b_k^\dagger + (g'/g)r_k(\hat{g})b_{-k}^\dagger)|GS\rangle \\ &+\frac{1}{1+(g'/g)^2} \sum_k \tilde{\phi}_k t_{2,k}(\hat{g})(a_{k'}^\dagger + (g'/g)b_{k'}^\dagger)|\text{exc}\rangle \end{aligned} \tag{15}$$

So the scattering amplitudes in the model with losses (denoted by the superscript ^{l}) are:

$$t_k^l(g) = \frac{1}{1+(g'/g)^2}(t_k(\hat{g}) + (g'/g)^2) \tag{16}$$

$$r_k^l(g) = \frac{1}{1+(g'/g)^2}\, r_k(\hat{g}) \tag{17}$$

$$t_{2,k}^l(g) = \frac{1}{1+(g'/g)^2}\, t_{2,k}(\hat{g}) \tag{18}$$

Figure 5 shows the results of calculations in two cases: $g = 0.12$, which is representative of a situation where counter-rotating terms are not playing an important role (panel b), and $g = 0.54$, as paradigmatic case of the ultra-strong regime (panel c). Panel (b) renders the elastic transmittance spectra for the case $g' = 0$, showing the null transmittance at resonance that appears when the qubit is lossless. The blue curve corresponds to $g' = g/2 = 0.06$, a value that has been chosen so that the transmission minimum is $\approx 6\%$, as in the experiments reported in [8], and the green one corresponds to $g' = 0.9g = 0.11$. The inset shows the fraction of energy that goes into the loss channel (the second waveguide). Panel (c) renders the transmittance for $g' = 0.06$, $g' = g/2 = 0.27$ and $g' = 0.9g = 0.48$, showing that the effect predicted in the main text is robust under dissipation. Even increasing the coupling into the loss channel to $g' = 0.9g$ preserves the main features found in the lossless case: a Fano resonance (with a minimum transmission that is not zero) and a high probability of Raman scattering (represented in the inset).

These results show that our predictions in the ultra-strong regime are expected to survive a moderate amount of dissipation, which can be even larger than that present in some actual realizations, as superconducting circuits.

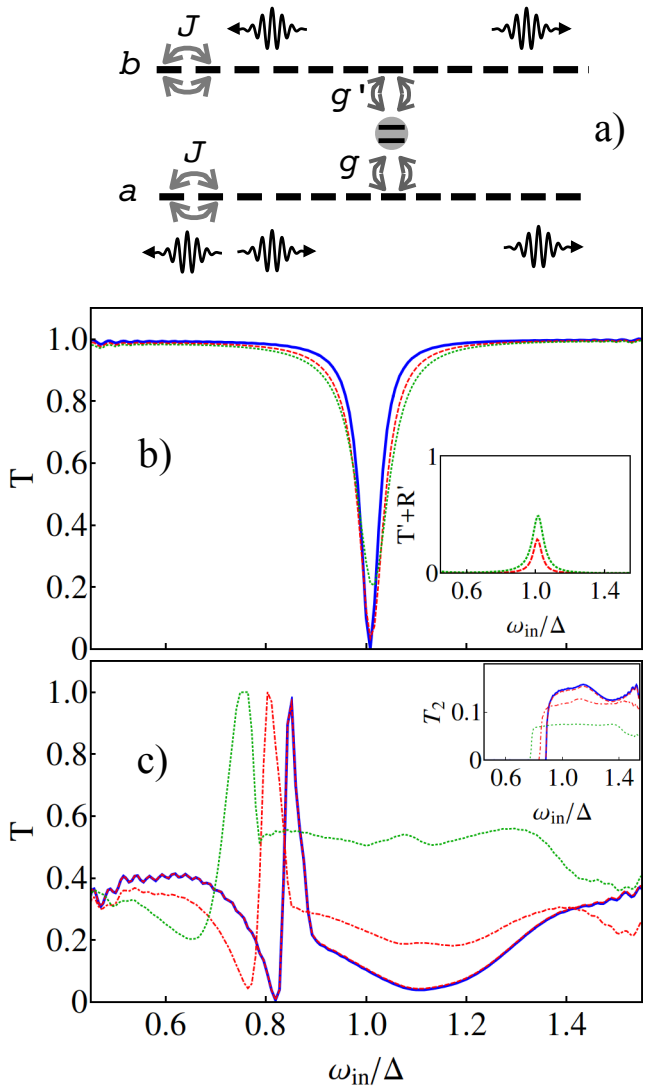

FIG. 7. Panel (a). Schematic representation of the geometry used for analyzing the effect of losses. Panel (b) Elastic transmittance spectrum for $g = 0.12$ and several g': 0 (continuous blue line), 0.06 (discontinuous red line) and 0.9 g = 0.11 (dotted green line). The inset shows the fraction of energy that goes into the upper waveguide. Panel (c) Elastic transmittance spectrum for $g = 0.54$ and g': 0 (continuous blue line), 0.06 (discontinuous red line), $g/2 = 0.27$ (dot-dotted red line), and $0.9g = 0.48$ (dotted greed line). In this panel the inset shows the fraction of inelastically transmitted energy.

VII. ABSENCE OF NONLINEAR SCATTERING IN LINEAR SYSTEMS

A. Linear models: Definition and first properties

Let us begin by defining a linear system:

Definition 1. *A linear model consists of a quadratic Hamiltonian of creation and annihilation bosonic operators ($[a_i, a_j^\dagger] = \delta_{ij}$, $[a_i, a_j] = 0$):*

$$H = \sum_{i,j} (\gamma_{i,j} a_i^\dagger a_j + (\beta_{i,j} a_i a_j + \text{hc})). \tag{19}$$

Here, the matrices γ and β define the Hamiltonian. Note that $\beta = 0$ implies RWA.

We order the set of bosonic operators such that a_i belongs to the chain if $1 \leq i \leq L$, whereas it corresponds to a scatterer if $i > L$. Therefore, we define $c_i := a_{L+i}$. Let us suppose there are M scatterers.

This Hamiltonian can be diagonalised within Bogolioubov-Valatin transformation

$$H = \sum \Lambda_l \alpha_l^\dagger \alpha_l, \tag{20}$$

up to an irrelevant constant, with $[\alpha_l, \alpha_m^\dagger] = \delta_{lm}$ and $\Lambda_l > 0$ for all l if the model is well behaved, with l going from 1 to $L + M$. The operators $\alpha_l^\dagger$ provide a simple representation of the ground state: $\alpha_l |GS\rangle = 0$, for all l. In addition, any eigenstate can be written as

$$|n_1, n_2, \ldots, n_{N_{cav}+M}\rangle = \frac{(\alpha_1^\dagger)^{n_1} (\alpha_2^\dagger)^{n_2} \ldots (\alpha_{N_{cav}+M}^\dagger)^{n_{N_{cav}+M}}}{\sqrt{n_1! n_2! \ldots n_{N_{cav}+M}!}} |GS\rangle \tag{21}$$

It is important to notice that the α's and the a's, are linearly related, and the relation is invertible

$$\alpha_l = \sum_{i=1}^{L} (\chi_{li}^a a_i + \eta_{li}^a a_i^\dagger) + \sum_{i=1}^{M} (\chi_{li}^c c_i + \eta_{li}^c c_i^\dagger). \tag{22}$$

Remark 1 The Hamiltonian (20) commutes with $N_\alpha = \sum \alpha_l^\dagger \alpha_l$. The number of excitations N_α turns to be a good quantum number. We will refer to it as α-particles or α-excitations.

Remark 2 The Hamiltonian (19) commutes with $P = \mathrm{e}^{i\pi \sum a_i^\dagger a_i}$, $[H, P] = 0$. P is called the parity operator. It means that the eigenstates of (20) are splitted in combinations of states with even number of particles and combinations of odd number of particles. E.g., the ground state is even. Trivially, the Hamiltonian also conserves the parity in the α's.

B. Scattering input

Let us consider a single-photon input state in momentum space

$$|\Psi_{in}\rangle = \sum_x \phi_x a_x^\dagger |GS\rangle = \sum_{k>0} \tilde{\phi}_k a_k^\dagger |GS\rangle, \tag{23}$$

with $\tilde{\phi}_k$ the Fourier transform of ϕ_x, so we have an incoming wavepacket exponentially distributed around k_{in}. Noting that the relation (22) is invertible, we can write a_i (or a_k), in terms of α_l and $\alpha_l^\dagger$. As $\alpha_l |GS\rangle = 0$, then the input state (23) in the α-representation will be

$$|\Psi_{in}\rangle = \sum_l \bar{\phi}_l \alpha_l^\dagger |GS\rangle, \tag{24}$$

where $\bar{\phi}_l$ is defined as

$$\sum_l \bar{\phi}_l (\tilde{\chi}_{lk}^a)^* = \tilde{\phi}_k, \tag{25}$$

with $\tilde{\chi}_{lk}^a$ the Fourier transform in the first index of χ_{li}^a. The input state (24) has got one α-particle.

C. No nonlinear scattering. A theorem

Theorem 1. *Given the single particle input state (24) there is not nonlinear scattering in linear optics: the output state is again a wavepacket with momentum k_{in} flying over the ground state.*

Proof. As the input state can be written as (24) and as N_α is a conserved quantity, the time evolution is restricted to the *one α-excitation level* (**remark 1**). Then the output state will be

$$|\Psi_{out}\rangle = \sum_l \bar{\phi}_l^{out} \alpha_l^\dagger |GS\rangle, \tag{26}$$

with $\bar{\phi}_l^{out} \equiv e^{-i\Lambda_l t_{out}} \bar{\phi}_l$. Writing this in terms of the initial operators (eq. 22), with those of the chain written in momentum space

$$|\Psi_{out}\rangle = \sum_l \bar{\phi}_l^{out} \left(\sum_k ((\tilde{\chi}_{lk}^a)^* a_k^\dagger + (\tilde{\eta}_{lk}^a)^* a_k) + \sum_i ((\chi_{li}^c)^* c_i^\dagger + (\eta_{li}^c)^* c_i) \right) |GS\rangle, \tag{27}$$

with $\tilde{\eta}_{lk}^a$ the discrete Fourier transform of η_{li}^a in the second index. This form of the output state (27) removes the possibility of having multiphoton scattering states; for instance, a two-photon state over the ground state would have terms like $a_{k_1}^\dagger a_{k_2}^\dagger |GS\rangle$. Then, the only possible scattering events are the elastic scattering, with transmission and reflection amplitudes t_k and r_k respectively, and a Raman process, where the scatterer does not come back to the ground state, but it remains in an excited state $|\text{exc}\rangle$. The photon emerges with a new momentum k_{new}, fulfilling energy conservation

$$\omega_{k_{in}} + E_{GS} = \omega_{k_{new}} + E_{\text{exc}} \tag{28}$$

This output state can be written as

$$|\Psi_{out}\rangle = \sum_{k>0} \tilde{\phi}_k (t_k a_k^\dagger + r_k a_{-k}^\dagger)|GS\rangle + \sum_k \tilde{\phi}_k^{new} a_k^\dagger |\text{exc}\rangle, \tag{29}$$

with $\tilde{\phi}_k^{new}$ a wavepacket centered around k_{new}. Writing the second term in α-operators:

$$\sum_k \tilde{\phi}_k^{new} a_k^\dagger |\text{exc}\rangle = \sum_l (\bar{\phi}_{l,+}^{new} \alpha_l^\dagger + \bar{\phi}_{l,-}^{new} \alpha_l)|\text{exc}\rangle, \tag{30}$$

Because of N_α and P conservation (**remarks 1** and **2**), $N_\alpha|\text{exc}\rangle = 2n|\text{exc}\rangle$ with $n \geq 1$. The first term of (30) will have $2n+1 \geq 3$ particles, and it is forbidden since $|\Psi_{out}\rangle$ has got just one α-particle, so this term vanishes.

Note that the energy of $\alpha_l|\text{exc}\rangle$ will be $E_{\text{exc}} - \Lambda_l$ (eqs. 20-21). Then, we are writing a term with energy $E_{\text{exc}} + \omega_{k_{new}}$ as a combination of states with energy $E_{\text{exc}} - \Lambda_l$, but it is a contradiction, because $E_{\text{exc}} + \omega_{k_{new}} > E_{\text{exc}} - \Lambda_l$. Then, the second term of (29) is not allowed, so the Raman process is forbidden too. This ends the proof. □

[1] B. Peropadre, D. Zueco, D. Porras, and J. J. García-Ripoll, Physical Review Letters **111**, 243602 (2013).
[2] J. Eisert, M. Cramer, and M. B. Plenio, Rev. Mod. Phys. **82**, 277 (2010).
[3] J. J. García-Ripoll, New Journal of Physics **8**, 305 (2006).
[4] F. Verstraete, V. Murg, and J. I. Cirac, Advances in Physics **57**, 143 (2008).
[5] B. Pirvu, V. Murg, J. Cirac, and F. Verstraete, New Journal of Physics **12**, 025012 (2010).
[6] M. Suzuki, Journal of Mathematical Physics **32**, 400 (1991).
[7] M. H. Devoret, in *Quantum Fluctuations*, edited by Les Houches Session LXIII (1995) pp. 351–386.
[8] O. Astafiev, A. M. Zagoskin, A. A. Abdumalikov, Y. A. Pashkin, T. Yamamoto, K. Inomata, Y. Nakamura, and J. S. Tsai, Science **327**, 840 (2010).